Inorganic Chemistry
Article
pubs.acs.org/IC

Rhombohedrally Distorted γ-$Au_{5-x}Zn_{8+y}$ Phases in the Au−Zn System

Srinivasa Thimmaiah* and Gordon J. Miller

Department of Chemistry, Iowa State University, and Ames Laboratory, U.S. Department of Energy, Ames, Iowa 50011, United States

Ⓢ *Supporting Information*

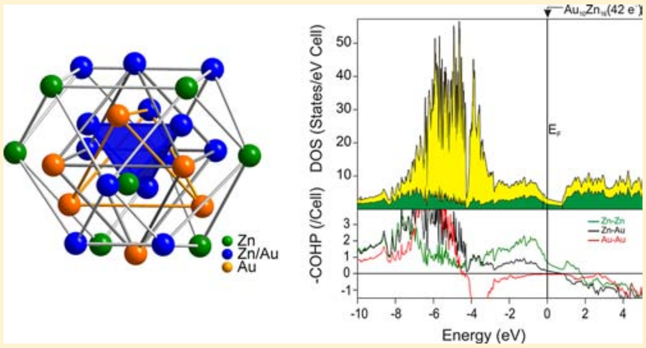

ABSTRACT: The region of the Au−Zn phase diagram encompassing γ-brass-type phases has been studied experimentally from 45 to 85 atom % Zn. The γ phases were obtained directly from the pure elements by heating to 680 °C in evacuated silica tubes, followed by annealing at 300 °C. Powder X-ray and single-crystal diffraction studies show that γ-"Au_5Zn_8" phases adopt a rhombohedrally distorted Cr_5Al_8 structure type rather than the cubic Cu_5Zn_8 type. The refined compositions from two single crystals extracted from the Zn- and Au-rich loadings are $Au_{4.27(3)}Zn_{8.26(3)}\square_{0.47}$ (**I**) and $Au_{4.58(3)}Zn_{8.12(3)}\square_{0.3}$ (**II**), respectively ($\square$ = vacancy). These (**I** and **II**) refinements indicated both nonstatistical mixing of Au and Zn atoms as well as partially ordered vacancy distributions. The structures of these γ phases were solved in the acentric space group $R3m$ (No. 160, $Z = 6$), and the observed lattice parameters from powder patterns were found to be $a = 13.1029(6)$ and 13.1345(8) Å and $c = 8.0410(4)$ and 8.1103(6) Å for crystals **I** and **II**, respectively. According to single-crystal refinements, the vacancies were found on the outer tetrahedron (OT) and octahedron (OH) of the 26-atom cluster. Single-crystal structural refinement clearly showed that the vacancy content per unit cell increases with increasing Zn, or valence-electron concentration. Electronic structure calculations, using the tight-binding linear muffin-tin orbital method with the atomic-sphere approximation (TB-LMTO-ASA) method, indicated the presence of a well-pronounced pseudogap at the Fermi level for "Au_5Zn_8" as the representative composition, an outcome that is consistent with the Hume−Rothery interpretation of γ brass.

■ INTRODUCTION

Research into Hume−Rothery γ-brass phases is experiencing a renaissance because of the numerous, emerging structure−composition relationships for these complex metallic alloys, which display some similarities with quasicrystalline solids.[1−3] Our own investigations into γ-brass phases of the Pd−Zn system revealed a complex intergrowth pattern of different sequences of fused icosahedra as a function of the valence electron concentration (vec) or electron-to-atom ratio (e^-/a).[4,5] Similar behavior occurs in the Fe−Zn,[6] Ni−Zn,[7] Rh−Zn[8] and Pt−Zn systems.[9] Subsequent modification of vec values in γ-brass Pd−Zn phases by introducing a third element, e.g., substituting trivalent Al for divalent Zn or monovalent Au for zerovalent Pd (just valence s and p electrons are counted),[10−12] yielded cubic γ-brass and 2 × 2 × 2 cubic superstructures, designated as γ' brass, in the Pd−Al−Zn[10,11] and Pd−Au−Zn[12] systems. These ternary γ- and γ'-brass phases exhibit directed mixed site occupancies as well as the presence of vacancies, both of which influence the vec of these phases to fall between 1.71 and 1.75 e^-/a. Corresponding electronic density of state (DOS) curves show that these vec values fix the Fermi levels to occur in pseudogaps, an effect that indicates Hume−Rothery-type behavior.[13−15] As part of this effort into the structural chemical behavior of γ brasses, we have also investigated the, as yet, unreported crystal structures of γ-brass phases in the Au−Zn binary system.

The Au−Zn binary phase diagram, shown in Figure 1, has been redrawn by Okamoto and Massalski using available experimental data.[16] According to this diagram, the Zn-rich regime consists of three distinct γ phases, namely, γ between 65 and 71 atom % Zn, γ_2 between 74 and 76 atom % Zn, and γ_3 between 81 and 83 atom % Zn at 300 °C.[16−18] Most of the experimental data were taken from work by Pearson.[18,19] In particular, the solidus and liquidus lines between 20 and 70 atom % Zn were established experimentally by Ipser and Krachler.[19] Furthermore, the γ_2 phase has the composition $AuZn_3$, the structure of which was confirmed by Günzel and Schubert.[20] The structure of the γ_3 phase was found to be hexagonal, but no crystal structure has been reported so far.[18] Pearson's work, on the other hand, was mainly motivated from previous results of Maciolek et al.,[21] who reported that the γ region of Au−Zn accommodated a single cubic phase with a large homogeneity range, i.e., 67−77 atom % Zn. This range corresponds to 86.8−92.0 valence s and p electrons per 52 atoms in the cubic unit cell. According to Pearson, these vec values (1.67−1.77 e^-/a) for the stability of the Au−Zn γ phases are significantly higher than those compared to typical γ brasses,[10] e.g., Cu_5Zn_8 (1.57−1.68 e^-/a), and would be susceptible to a rhombohedral distortion, as in Cr_5Al_8.[22]

Received: September 4, 2012
Published: January 16, 2013

dx.doi.org/10.1021/ic301933a | *Inorg. Chem.* 2013, 52, 1328−1337

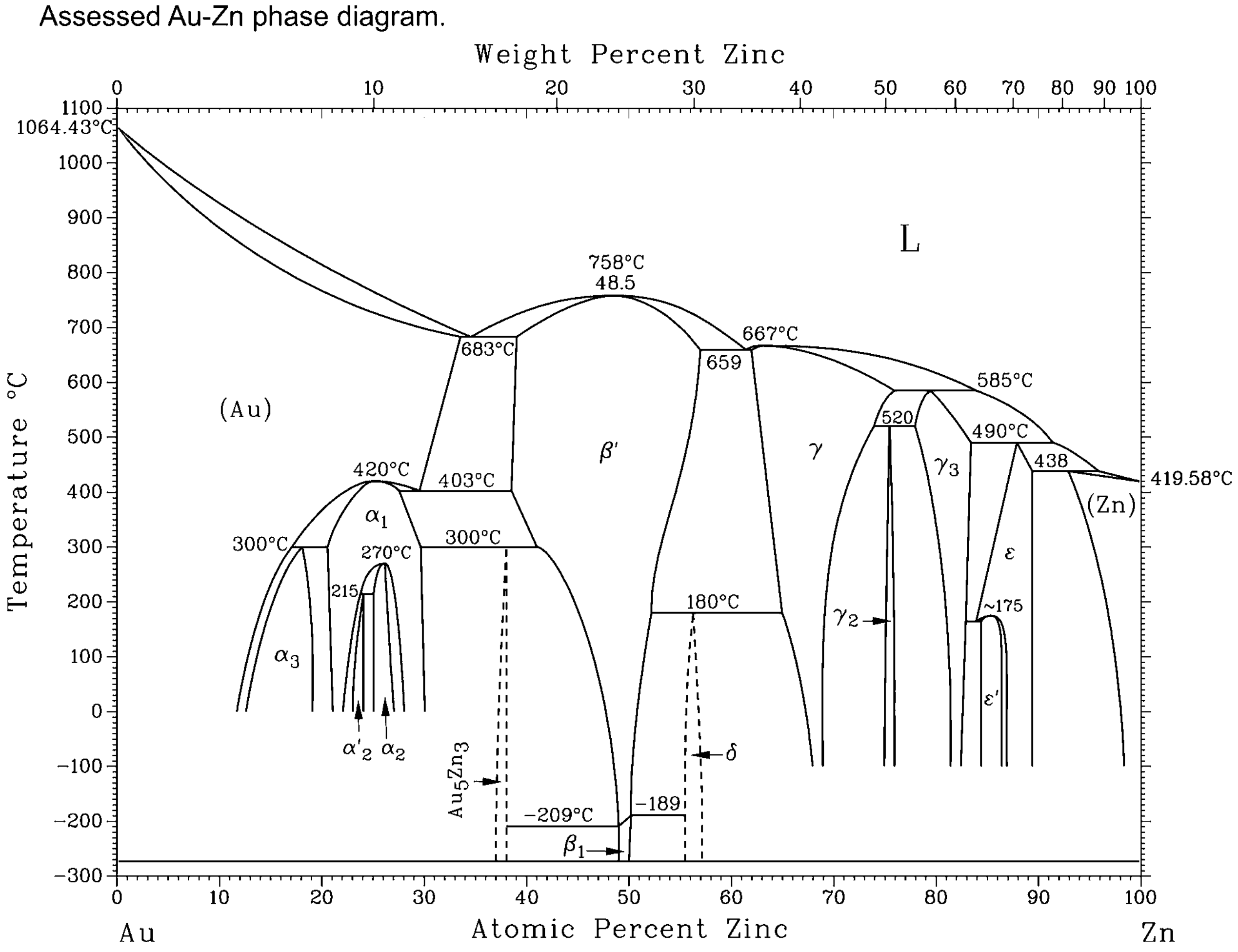

Figure 1. Au−Zn phase diagram taken from Okamoto and Massalski.[16]

Consequently, Pearson redetermined the Au−Zn phase diagram to identify the phase width and crystal structures of the γ-brass phases.[18] He concluded the existence of only the cubic γ phase between 65 and 71 atom % Zn at 300 °C and extended its homogeneity range between 68 and 69 atom% Zn at room temperature. All previous reports, including Pearson's work, conclude that the Au−Zn γ phase adopts the cubic Cu_5Zn_8 structure type with a noticeable phase width.[16,18,21,23] However, our experimental results indicate that the Au−Zn γ phase adopts a rhombohedrally distorted γ-brass-type structure and exists for a relatively narrow range of chemical compositions, and, thus, vec values.

Rhombohedrally distorted γ-brass-type structures have been reported for many binary systems (Table 3), namely, T−Ga (T = Cr,[24] Fe,[24] and Mn[25]), T−Al (T = Cr,[22] Mn,[26] and Cu[27]), and Cu−Hg systems.[28] So far, all of the reported distorted γ-brass phases have a rhombohedral cell angle α of less than 90° except for Cu_7Hg_6, which has an α greater than 90°. According to Pearson's speculations, the rhombohedral distortion from cubic symmetry at higher vec values is driven by lowering the band structure energy.[22] Recently, we also reported the structures and magnetic properties of MGa (M = Cr, Mn, and Fe)[24,25] and pseudobinary $Cr_{1-x}Fe_xGa$ systems,[29] which are, in fact, rhombohedrally distorted γ-brass-type structures. The net magnetization along these series from Cr to Fe changes from weakly antiferromagnetic to ferromagnetic. In addition, all of these phases show a broad partially filled d band that can obscure accurate assessment of a sp-based vec. Interestingly, the distorted γ-brass compounds MGa (M = Cr, Mn, and Fe)[24,25] adopt a centrosymmetric space group ($R\bar{3}m$) rather than a noncentrosymmetric space group, as observed for Cr_5Al_8 or Cu_6Hg_7 ($R3m$).

The main focus of this report, therefore, is to establish the crystal structures of previously unreported γ-brass-type structures in the Au−Zn phase diagram. As part of the goal, we also explored the phases between 45 and 85 atom % Zn to identify the phase width of γ phases and also the crystal structures of neighboring phases. Moreover, we include an analysis of the electronic structure of γ-Au_5Zn_8.

■ EXPERIMENTAL SECTION

Synthesis and Analysis. Several different Au−Zn samples ranging from 45 to 85 atom % Zn were targeted by combining the pure elements, Au [99.99%, Material Preparation Center (MPC), Ames Laboratory] and Zn (99.999%, MPC, Ames Laboratory). A complete listing of loaded compositions is provided in the Supporting Information (Table S1). The pure elements of these targeted compositions were sealed in evacuated silica tubes under vacuum (10^{-5} Torr), heated continuously from ambient temperature to 680 °C at a heating rate of 30 °C/h, and held there for 12 h. The reaction mixtures were then cooled to 300 °C at a cooling rate of 200 °C/h, at which point the samples were equilibrated for 5 days. Finally, the silica tubes were quenched in cold water.

To examine the phase purity and verify any homogeneity range, all samples were examined by powder X-ray diffraction (XRD) using a Philips PANalytical X'Pert PRO diffractometer. The samples were mounted on specially cut single-crystal silicon and spread evenly with the aid of laboratory-grade acetone. The data were collected for 2θ values ranging from 10° to 90° at increments of 0.02° in a continuous scan mode using Cu Kα radiation (λ = 1.540598 Å) in Bragg−Brentano geometry. The lattice parameters were refined using the *WINXPOW* program.[30]

Semiquantitative microprobe analyses were performed on several single crystals using a JEOL 5910LV scanning electron microscope equipped with a Noran-Vantage energy-dispersive spectrometer. To achieve more accurate compositions, samples were embedded in the epoxy and carefully polished to obtain a flat surface. The energy-dispersive X-ray spectrometry (EDS) spectra were acquired using an accelerating voltage of 20 keV. Images were also taken in the backscattered electron mode to check for the presence of any additional phases. The chemical compositions obtained from EDS corroborate well with refinements from single-crystal data analysis, within the limitations of the technique. No heavy elements other than Zn and Au were detected.

Differential Scanning Calorimetry (DSC). Thermal analyses were performed on a Netzsch DSC 404 C thermal analyzer. Approximately 40−60 mg of crystalline material (a chunk) was placed into a Ta tube with a 4 mm outer diameter. The Ta tube was evacuated in the special container and then sealed using a plug of Ta wire with the aid of a Nd:YAG laser (Miycachi Unitek LW150A) under vacuum (10^{-5} Torr). The samples were heated to 800 °C at a heating rate of 10−20 °C/min and then cooled to room temperature at a cooling rate of 10−20 °C/min. These cycles were repeated at least twice to ensure reproducibility.

Single-Crystal Structure Determination. Several suitable single crystals were selected from various samples to corroborate the phase width and to examine the element distributions for the Au−Zn γ brasses. All crystals were studied using a Bruker APEX CCD diffractometer equipped with graphite-monochromatized Mo Kα radiation (λ = 0.71073 Å). Herein, we report detailed structural refinement of two specimens extracted from Zn-rich (**I**: $Au_{4.5}Zn_{8.5}$, loaded composition) and Au-rich (**II**: Au_5Zn_8, loaded composition) samples. All refined compositions of the remaining crystals fall between these two extremes, and some of these results are summarized in Table 5. Reflections were gathered at room temperature by taking three sets of 606 frames with 0.3° scans in ω, with an exposure time of 15−20 s/frame using the *SMART* program.[31] The range of 2θ extended from 4 to 57°. The measured intensities were corrected for Lorentz and polarization effects. The intensities were further corrected for absorption using the program *SADABS*, as implemented in *SHELXTL+*.[32] All data sets showed the systematic absence condition hkl: $-h + k + l = 3n$, etc., which suggests rhombohedral symmetry and five possible space groups, $R\bar{3}$, $R3$, $R3m$, $R32$, and $R\bar{3}m$. The *E*-Stats model strongly suggested the structures to be centrosymmetric; consequently, the space group $R\bar{3}m$ was tentatively chosen for structural refinement. However, to establish structural relationships to the known rhombohedrally distorted γ-brass-type structures, the structures were also refined in the noncentrosymmetric space group $R3m$, a strategy that provided better refinement statistics.

Centrosymmetric Refinement for Crystal I. In the centrosymmetric space group $R\bar{3}m$, direct methods yielded an initial asymmetric unit with four Zn positions and two Au positions, according to their thermal displacement parameters. Subsequent isotropic least-squares refinement cycles converged quickly to R1 = 15.9%. The thermal displacement parameters for three of the four Zn positions were well behaved, while the fourth position showed negative displacement parameters. This position was tentatively assigned as Au in the subsequent refinement cycle. In addition, relatively large displacement parameters were observed for the two Au positions. Therefore, in the final refinement cycles, three positions were treated as mixed Au/Zn, and the R1 values converged to 11%. In the following least-squares cycles, the occupancy parameters were refined for the remaining Zn2, Zn5, and Au4 positions to obtain the refined composition. The occupancy of both Zn sites settled around 100% (within 3σ), whereas the Au4 site refined to 86(2)% occupied. The final stages of refinement were carried out with anisotropic displacement parameters and yielded R1 = 5.65% for 34 parameters. The final refined composition from this centrosymmetric model is $Au_{4.33(3)}Zn_{8.26(3)}\square_{0.41}$.

Noncentrosymmetric Refinements for Crystals I and II. Subsequent refinement for crystal **I** in the noncentrosymmetric space group $R3m$ yielded nine crystallographically independent positions. During the early stages of structural refinement, four of these were assigned to Au and the remaining ones were assigned to Zn, which resulted in R1 dropping to 13%. The displacement parameters for three of the five assigned Zn positions showed negative values; on the other hand, three out of the four Au positions showed relatively large displacement parameters. This indicates a possible mixing of Au/Zn on six different atomic positions. In the subsequent refinement cycle, these positions were assigned as mixed Au/Zn positions, as a result of which the *R* value dropped to 9%. To obtain an accurate composition, the occupancy parameters were refined in a separate series of least-squares cycles. All independent Zn positions show full occupancy (within 3σ); however, the Au4 and Au6 positions show deviations from full occupancy, suggesting vacancies or admixing with Zn on these sites. However, when the Au4 and Au6 sites were treated as mixed Au/Zn positions, no Zn accumulated on these positions. Eventually, these two positions are most successfully refined as partially occupied Au sites and the refined occupancies for Au4 and Au6 are 94(1)% and 86(1)%, respectively. It is noteworthy that the Zn1 position shows a relatively large equivalent isotropic displacement parameter compared to other positions; however, the occupancy was refined to unity within 3σ. The final stages of refinement were carried out using anisotropic displacement parameters and yielded R1 = 3.9% for 60 parameters. The refined composition in this noncentrosymmetric model was found to be $Au_{4.58(3)}Zn_{8.12(3)}\square_{0.3}$, which is in agreement with EDS analysis (EDS = $Au_{38(2)}Zn_{62(2)}$ = $Au_{4.9(2)}Zn_{8.1(2)}$), and differs slightly from the centrosymmetric refinement ($Au_{4.33(3)}Zn_{8.26(3)}\square_{0.41}$). Hamilton's significance test suggests that the noncentrosymmetric model is statistically better at the 95% confidence level than the centrosymmetric model.[33]

Crystal **II** was extracted from the Zn-rich loading "$Au_{4.5}Zn_{8.5}$" and coexists with an unknown phase, according to our observed powder XRD pattern. Its starting parameters were taken from the results of crystal **I**. After a few cycles of isotropic refinement, the R1 value dropped to 9.3%. In the following steps, the occupancy parameters were refined just for the Zn1, Zn8, Au4, and Au8 positions. The occupancy of the Zn positions settled around 100% (within 3σ), whereas the Au4 and Au6 positions were refined to 84(2)% and 85(1)%, respectively. The final stages of refinement were carried out with anisotropic displacement parameters and yielded R1 = 5.1% for 60 parameters. The refined composition was found to be $Au_{4.27(2)}Zn_{8.26(2)}\square_{0.47}$, which is in good agreement with EDS analysis (EDS = $Au_{33(2)}Zn_{67(2)}$= $Au_{4.3(2)}Zn_{8.7(2)}$). Although the equivalent isotropic thermal displacement parameters for the Zn1 and Zn8 sites are relatively high, no vacancies could be refined on these sites. Tables 1 and 2 summarize the atomic positions, site occupancy factors, and displacement parameters for crystals **I** and **II**.

RESULTS AND DISCUSSION

Our synthetic and crystallographic investigation of the Au−Zn system in the approximate range 45−85 atom % Zn reveals the existence of a rhombohedrally distorted γ-brass-type phase and other phases. The distorted γ-brass-type "Au_5Zn_8" phase was observed between 58.0 and 69.0 atom % Zn at 300 °C. Our results contradict previous reports,[12,14−16,30] which suggest that the Au_5Zn_8 phase adopts the cubic γ-Cu_5Zn_8-type structure. Powder XRD analysis (see Figure 2) indicated the presence of small amounts of a secondary phase (unknown or β') in most of the samples depending on the loaded compositions. Single-crystal diffraction studies on several crystals show the presence of a small homogeneity range for the γ phase, as well as the presence of vacancies on Au sites and admixing of Au/Zn on several crystallographic sites. Furthermore, a new phase with

Table 1. Crystallographic Data for Crystals I, Extracted from Loaded Composition Au_5Zn_8, and II, Extracted from the Loaded Composition $Au_{4.5}Zn_{8.5}$.

	I	II
empirical formula	$Au_{4.58(3)}Zn_{8.12(3)}\square_{0.3}$	$Au_{4.27(3)}Zn_{8.26(3)}\square_{0.47}$
fw	1432.15	1380.67
wavelength (Å)	0.71073	0.71073
cryst syst, space group	rhombohedral, $R3m$ (No. 160)	rhombohedral, $R3m$ (No. 160)
unit cell dimens		
a (Å)	13.1345(8)	13.1029(6)
c (Å)	8.1103(6)	8.0410(4)
volume (Å^3); Z	1211.70(14); 6	1195.57(10); 6
calcd density (g/cm^3)	11.776	11.506
abs coeff (mm^{-1})	106.275	102.477
F(000)	3631	3510
cryst size (mm^3)	0.03 × 0.06 × 0.12	0.03 × 0.07 × 0.10
θ range (deg)	3.08–28.24	3.08–28.24
limiting indices	$-17 \leq h \leq 17, -16 \leq k \leq 16, -10 \leq l \leq 10$	$-16 \leq h \leq 17, -17 \leq k \leq 16, -10 \leq l \leq 10$
reflns collected/unique	3571/732 [R(int) = 0.0444]	3535/720 [R(int) = 0.0692]
refinement method	$\|F\|^2$	$\|F\|^2$
data/param	732/60	720/60
GOF on $\|F\|^2$	1.028	1.101
final R indices [$I > 2\sigma(I)$]	R1 = 0.0398, wR2 = 0.0773	R1 = 0.0513, wR2 = 0.0995
R indices (all data)	R1 = 0.0527, wR2 = 0.0840	R1 = 0.0691, wR2 = 0.1068
absolute structure param	0.44(5)	0.46(7)
largest diff peak and hole (e/Å^3)	1.985 and −3.725	2.049 and −3.134

Table 3. Structure of Rhombohedrally Distorted γ Phases Reported for Different Binary Systems

phase	lattice parameters (pseudocubic)	angle, α (deg)	space group	reference
Cr_5Al_8	9.057(6)	89.28(5)	$R3m$	59
Mn_5Al_8	9.1706(2)	89.09(1)	$R3m$	26
$Cu_{7.8}Al_5$	8.6899(9)	89.78(1)	$R3m$	27
Cu_7Hg_6	9.4076(7)	90.41(1)	$R3m$	28
$Au_{5-x}Zn_{8+y}$	9.3565(4)	89.72(2)	$R3m$	this work
CrGa	8.9893(2)	89.73(2)	$R\bar{3}m$	24
MnGa	9.2866(3)	88.41(2)	$R\bar{3}m$	25
FeGa	8.9653(3)	89.26(2)	$R\bar{3}m$	24

approximate unit cell composition $Au_{72.5}Zn_{150}$ was observed between the γ and γ_2 phases. This phase crystallizes in its own structure type, adopting trigonal symmetry. The existence of the γ_2 phase was reconfirmed by single-crystal XRD studies, yielding a refined composition of $AuZn_3$, which agrees with earlier results.[20] In addition, DSC analyses show that the γ phase melts around 661 °C, which is consistent with the previously reported phase diagram by Okamoto and Massalski.[16]

Phase Analysis. Powder XRD data were acquired on various samples to examine the phase width of $Au_{5-x}Zn_{8+y}$ ($1 \geq x \geq -0.5$), which ranges from approximately 58 to 69 atom % Zn. The unknown phase was the major phase observed in the range $1 \geq x \geq 0.5$ (65–69 atom % Zn). A single-crystal diffraction study on the unknown phase revealed that its structure crystallizes in trigonal symmetry with lattice parameters a = 22.677(4) Å and c = 7.999(2) Å. On the basis of the single-crystal structure refinement, the approximate composition of the new phase is $Au_{72.5}Zn_{150}$ and will be the subject of a future report (Figure S6 in the Supporting Information).[34] Samples loaded in the composition range $0.5 \geq x \geq -0.5$ (58–65 atom % Zn) contained γ brass as the major product along with noticeable amounts of a secondary β' phase (CsCl, body-centered-cubic type).[35] EDS analysis yielded the composition of this secondary phase to be $Au_{0.5}Zn_{0.5(3)}$. A representative SEM micrograph, shown in the Supporting Information (Figure S1), for loaded composition Au_5Zn_8 illustrates this outcome. Furthermore, as the loaded Au content increases, there is a substantial increase in the amount of the β' phase in the product. The enrichment of the β phase can be clearly seen in the SEM micrograph (see the Supporting

Table 2. Atomic Coordinates and Equivalent Isotropic Displacement Parameters (Å^2) for Crystals I and II (Bold)[a]

	atom	Wyckoff site	occupancy	x	y	z	U_{eq}
IT(1)	Zn1	3a	1	0	0	0.1930(23)	0.040(2)
			1	**0**	**0**	**0.1689(24)**	**0.047(4)**
IT(3)	Zn/Au2	9b	0.76/0.24(1)	0.4175(2)	0.5825(2)	0.6041(5)	0.024(1)
			0.94/0.06(1)	**0.4212(3)**	**0.5788(3)**	**0.6086(6)**	**0.026(2)**
OT(1)	Zn/Au3	3a	0.39/0.61(2)	0	0	0.7031(11)	0.025(1)
			0.41/0.59(2)	**0**	**0**	**0.7202(7)**	**0.022(2)**
OT(3)	Au4	9b	0.93(1)	0.5455(1)	0.4545(1)	0.4679(2)	0.024(1)
			0.84(2)	**0.5456(1)**	**0.4544(1)**	**0.4669(3)**	**0.026(1)**
OH(3)	Zn/Au5	9b	0.70/0.30(2)	0.5500(2)	0.4500(2)	0.1065(5)	0.022(2)
			0.82/0.18(2)	**0.5505(2)**	**0.4495(2)**	**0.1028(7)**	**0.031(2)**
OH(3′)	Au6	9b	0.87(1)	0.4514(1)	0.5487(1)	0.9294(2)	0.021(1)
			0.85(1)	**0.4514(1)**	**0.5486(1)**	**0.9283(3)**	**0.027(1)**
CO(3)	Zn/Au7	9b	0.88/0.12(1)	0.5863(3)	0.4137(3)	0.7904(6)	0.025(2)
			0.79/0.21(2)	**0.5871(2)**	**0.4129(2)**	**0.7963(6)**	**0.029(2)**
CO(3′)	Zn/Au8	9b	0.61/0.39(2)	0.4523(1)	0.5477(1)	0.2874(5)	0.024(1)
			0.50/0.50(2)	**0.4533(2)**	**0.5467(2)**	**0.2860(4)**	**0.030(1)**
CO(6)	Zn9	18c	1	0.3035(4)	0.3363(5)	0.0444(12)	0.031(1)
			1	**0.3063(4)**	**0.3393(5)**	**0.0522(12)**	**0.049(2)**

[a] U_{eq} is defined as one-third of the trace of the orthogonalized U_{ij} tensor.

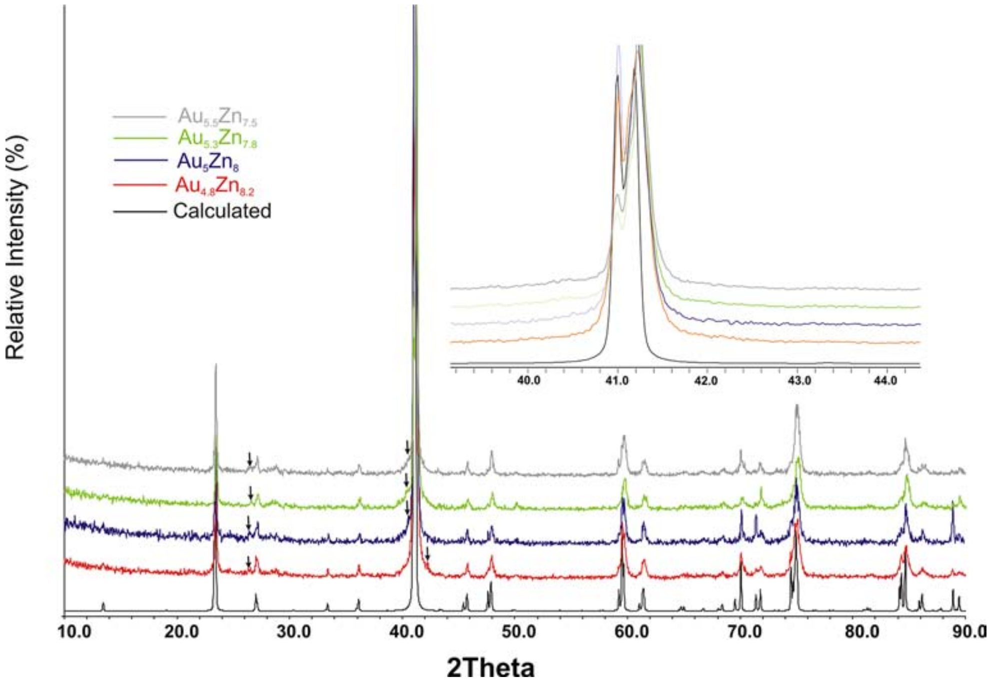

Figure 2. Powder XRD diffractogram for various loaded compositions. Most of the samples show a small amount of the β' phase, indicated by arrows.

Information, Figure S2). However, the powder XRD patterns presented in Figure 2 do not account for all of the β' phases because the β' phase is ductile and can be easily separated mechanically from the γ phase. Thus, only small amounts of a β' phase were detected in the powder XRD patterns containing higher amounts of Au ($0.2 > x > -0.5$; i.e., 58−60 atom % Zn). Using our synthetic conditions, γ phases were never obtained as single-phase products. As described in the Experimental Section, our reaction mixtures were typically cooled from the melt to access better quality single crystals for diffraction studies. Although the reaction mixtures were quickly cooled to obtain the desired γ phase, some amount of β' or unknown phases was always observed in the powder XRD patterns, depending upon the loaded compositions. These results agree with the experimental work by Ipser and Krachler[19] and the thermodynamic assessments of Liu et al.[23]

A careful analysis of several powder XRD diffractograms within the γ-brass region also revealed the splitting of several reflections, including the main reflection around 41° in 2θ, a result that indicates distortion of the structure from cubic symmetry. Figure 2 shows the powder XRD patterns of several loaded compositions. These results disagree with previous reports that reported a cubic γ-brass-type structure but do corroborate Pearson's speculation arising from chemical compositions. Lattice parameters refined from the powder XRD patterns yield unit cell volumes ranging from 1195.6(4) Å^3 for the most Zn-rich sample (refined composition of $Au_{4.27(3)}Zn_{8.26(3)}$; ∼66 atom % Zn) to 1211.7(3) Å^3 for the most Au-rich γ phase (refined composition of $Au_{4.84(3)}Zn_{7.85(3)}$; ∼62 atom % Zn). Variation of the cell volume with respect to the Zn (loaded) is shown in Figure 3. According to the figure, the γ-brass cell volumes are nearly constant between 58 and 61.5 atom % Zn; i.e., the composition of the γ phase does not change in this region. As mentioned before, this is a two-phase region ($\beta' + \gamma$) in which β' is the major phase. The volume shows a downward trend with increasing Zn content starting from 61.5 atom % and extending up to 65.5 atom % Zn. Further increasing the Zn content leads to formation of $\gamma$the $_2$ phase. The powder XRD diffractogram obtained from the sample containing 67 atom % Zn ("$Au_{4.3}Zn_{8.7}$") shows the presence of nearly a single phase of $Au_{72.5}Zn_{150.}$ Therefore, on the basis of combined single-crystal diffraction and EDS studies, the upper and lower boundaries of the γ phase are assigned between 62.0 and 66.0 atom % Zn at 300 °C.

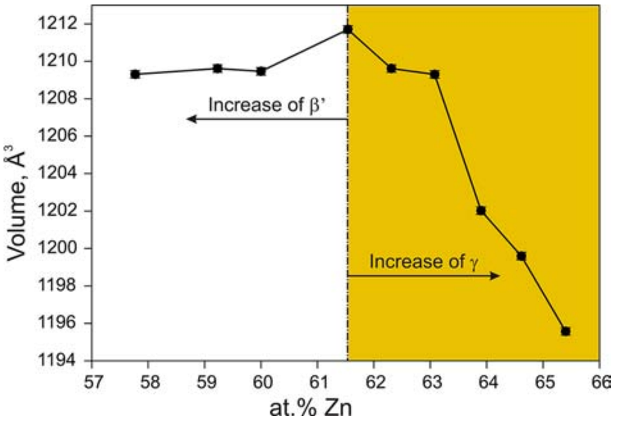

Figure 3. Variation of the cell volumes for rhombohedrally distorted γ-$Au_{5-x}Zn_{8+y}$ samples with respect to the loaded composition.

Thermal Analysis. To assess the phase width of the γ phase apart from the powder XRD and single-crystal diffraction studies, DSC analyses were conducted for three loaded compositions, namely, $Au_{4.6}Zn_{8.4}$ (64.6 atom % Zn), Au_5Zn_8 (61.5 atom % Zn), and $Au_{5.3}Zn_{7.7}$(59.2 atom % Zn). These three samples represent the Zn-richest, an intermediate, and the Zn-poorest compositions for which the γ phase has been observed as the major phase. Even though powder XRD patterns show the presence of small amounts of secondary phases such as $Au_{72.5}Zn_{150}$ coexisting with $Au_{4.6}Zn_{8.4}$ and β'

with $Au_{5.3}Zn_{7.7}$, the γ phase can be mechanically separated for $Au_{4.6}Zn_{8.4}$ and Au_5Zn_8 loaded compositions. However, a small amount of the β' phase has been observed in the thermal event for $Au_{5.3}Zn_{7.7}$ (Table 4). During the first heating cycle, an endothermic signal corresponds to melting of the γ phase at onset temperatures of 657 and 667 °C respectively for $Au_{4.6}Zn_{8.4}$ and Au_5Zn_8. Upon cooling, an exothermic signal corresponds to recrystallization of the γ phase at temperatures 660 and 668 °C (onset) respectively for $Au_{4.6}Zn_{8.4}$ and Au_5Zn_8. No additional signals were observed. Similar types of events were observed for both $Au_{4.6}Zn_{8.4}$ and Au_5Zn_8 samples, during the second heating cycle (see the Supporting Information). Our experimental results agree very well with the previously reported (667 °C, melting temperature of the γ phase) phase diagram by Okamoto and Massalski.[16]

Table 4. Thermal Events Observed for the Three Loaded Compositions in the γ-Phase Region (Onset Temperatures Are Given)[a]

loaded composition	Ist HC/°C		Ist CC/°C		IInd HC/°C		IInd CC/°C	
	I	II	I	II	I	II	I	II
$Au_{4.6}Zn_{8.4}$	660		668		663		665	
Au_5Zn_8	657		660		657		659	
$Au_{5.2}Zn_{7.8}$	661	696	657	703	663	700	656	704

[a] HC = heating cycle. CC = cooling cycle. I-event corresponds to the γ phase, and II-event corresponds to the β' phase.

On the other hand, the first heating and cooling cycle at a rate of 10 °C/min of loaded composition $Au_{5.2}Zn_{7.8}$ shows two events. Upon heating, the first event corresponds to melting of the γ phase at 661 °C, and the second broad endothermic peak corresponds to the melting point of a β' phase with an onset temperature of 696 °C (maximum at 705 °C). During the cooling cycle, a relatively sharp single peak corresponds to recrystallization of the β' phase at an onset temperature of 703 °C, followed by a second exothermic event at 658 °C, which corresponds to recrystallization of the γ phase. A second heating and cooling cycle at 10 °C/min of the $Au_{5.2}Zn_{7.8}$ sample gives reproducible results. When larger scan rates were employed (e.g., 15 °C/min), formation of the γ phase could not be observed upon cooling. The thermograms for the loaded compositions for Au_5Zn_8 and $Au_{5.2}Zn_{7.8}$ are shown in Figure 4. The observed temperature ranges for melting and recrystallization of the β' phase show excellent agreement with the temperature ranges recently reported by Ipser and Krachler.[19]

Structural Analysis. Single-crystal diffraction and powder XRD studies on several samples show that the Au−Zn γ phase adopts a distorted Cr_5Al_8 γ-brass-type structure. Crystals **I** and **II**, which were selected from loaded samples such as "Au_5Zn_8" and "$Au_{4.5}Zn_{8.5}$", are best refined in the noncentrosymmetric space group $R3m$ ($Z = 6$) and show slight differences in their refined compositions, i.e., $Au_{4.58(3)}Zn_{8.12(3)}\square_{0.3}$ for **I** and $Au_{4.27(3)}Zn_{8.26(3)}\square_{0.47}$ for **II**. However, the most Au-rich γ phase found in this series gave a refined composition of $Au_{4.84(3)}Zn_{7.85(3)}\square_{0.31}$, which was extracted from the loaded composition of $Au_{5.3}Zn_{7.7}$. The R1 value for this Au-rich crystal was slightly higher (R1 = 0.0694/wR2 = 0.1318) compared to crystals **I** and **II**. In addition, the M5 position was refined isotropically because anisotropic refinement yielded a non-positive definite result, thus indicating possible absorption problems. Nevertheless, the structural models yielded identical sites for Au/Zn mixing. The compositions from single-crystal refinement results from different crystals are tabulated in Table 5.

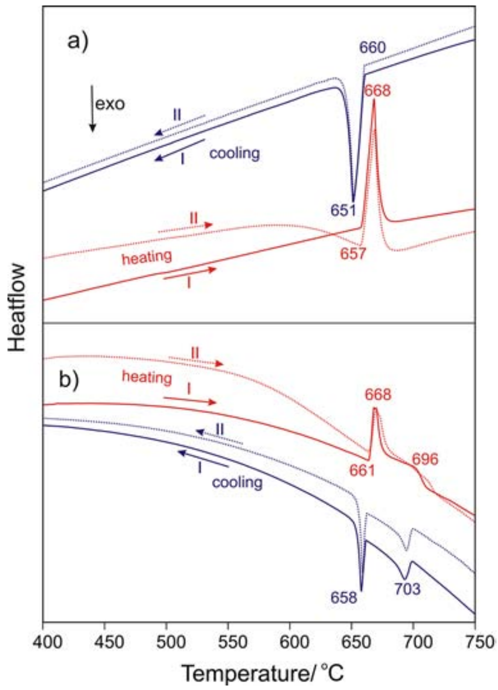

Figure 4. DSC traces for Au_5Zn_8 (a) and $Au_{5.2}Zn_{7.8}$ (b) loaded compositions. Exotherms and endotherms are identified by their onsets and maximum peak heights. The heating and cooling rates are 10−20 °C/min.

Table 5. Results from Single-Crystal Structural Refinement for Four Different Crystals Extracted from Different Loaded Compositions along with Their Corresponding Residual R1/wR2 Values and EDS Results

no.	loaded composition	refined composition	R1/wR2	EDS results
I	$Au_{4.5}Zn_{8.5}$	$Au_{4.27(3)}Zn_{8.26(3)}\square_{0.47}$	0.0513/0.0995	$Au_{4.1(3)}Zn_{8.4(3)}$
	$Au_{4.8}Zn_{8.2}$	$Au_{4.42(3)}Zn_{8.19(3)}\square_{0.39}$	0.0602/0.1046	$Au_{4.4(2)}Zn_{8.2(2)}$
II	Au_5Zn_8	$Au_{4.58(3)}Zn_{8.12(3)}\square_{0.30}$	0.0398/0.0773	$Au_{4.8(3)}Zn_{7.9(3)}$
	$Au_{5.3}Zn_{7.7}$	$Au_{4.84(3)}Zn_{7.85(3)}\square_{0.31}$	0.0694/0.1318	$Au_{5.1(3)}Zn_{7.6(3)}$

A group−subgroup relationship can be established by relating the cubic γ-Cu_5Zn_8 aristotype to the rhombohedrally distorted γ-$Au_{5-x}Zn_{8+y}$ structure to understand the distribution of Au and Zn atoms within the 26-atom γ-brass cluster. The symmetry reduction from $I\bar{4}3m$ to $R3m$ involves a *klassengleich*-type group reduction of index 4 with a 3 times enlarged cell, i.e., $I\bar{4}3m \rightarrow k4\ [a' = -a + b,\ b' = -b + c, \text{ and } c' = {}^1/_2(a + b + c)] \rightarrow R3m$. The group−subgroup relationships and evolution of the corresponding atomic positions are summarized in Figure 5 as a *Bärnighausen* tree.[36,37]

The cubic γ-brass structure consists of two 26-atom γ clusters,[38] packed in a body-centered-cubic fashion. Each γ cluster can be decomposed into four successive polyhedral shells consisting of (i) an inner tetrahedron (IT) of four atoms, (ii) an outer tetrahedron (OT) of four atoms, (iii) an

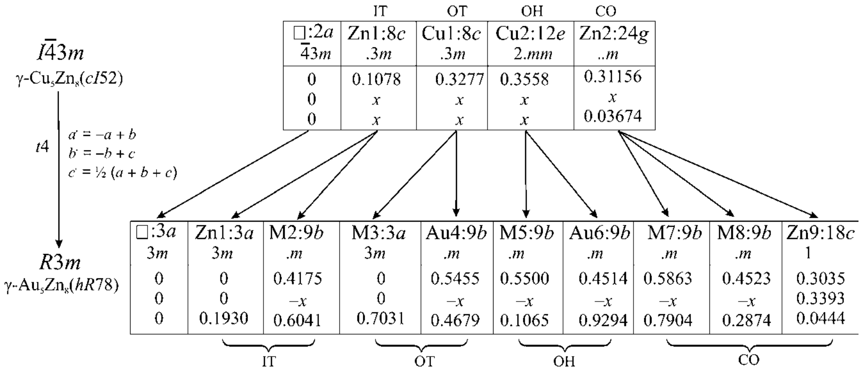

Figure 5. Group−subgroup relationship (*Bärnighausen* tree) between the atristotype γ-Cu$_5$Zn$_8$ and rhombohedrally distorted γ-Au$_5$Zn$_8$.

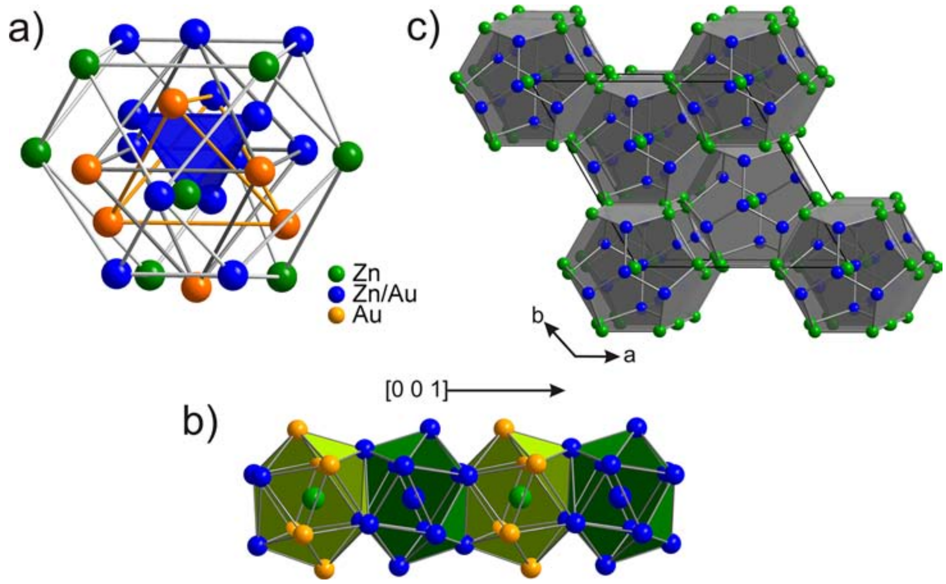

Figure 6. Different representations of the γ-Au$_5$Zn$_8$ structure: (a) 26-atom cluster displaying successive shells of atoms; (b) chain of face-shared icosahedra along the *c* axis, centered by Zn1 and M3 atoms; (c) 3D network of Zn1-centered pentagonal dodecahedra: inner icosahedra are omitted for clarity.

octahedron (OH) of six atoms, and (iv) a distorted cuboctahedron (CO) of 12 atoms. In cubic γ brasses, these γ clusters have $\bar{4}3m(T_d)$ symmetry.[38] This structural description has been effectively used for numerous γ, γ', and other distorted γ-brass phases[10,12,14,22,39−41] and has yielded exceptional insights about the structural chemistry and atomic distributions in γ brasses, in general.

For rhombohedrally distorted γ-Au$_{5-x}$Zn$_{8+y}$, the γ clusters adopt $3m(C_{3v})$ symmetry, shown in Figure 6a. The Zn1 (3a) and M2 (9b) atoms form the IT, surrounded by the OT of M3 (3a) and Au4 (9b) atoms. This is enclosed by an OH made up of three Zn5 (9b) and three M6 (9b) sites and is further encased by a CO composed of three Au7 (9b), three M8 (9b), and six Zn9 (18c) positions. According to the single-crystal structural refinements, the vacancies are observed at the two Au sites located on the OT and OH sites. As a result, the overall refined compositions are Au$_{4.27(3)}$Zn$_{8.26(3)}\square_{0.47}$ and Au$_{4.58(3)}$Zn$_{8.12(3)}\square_{0.3}$ ($\square$ = vacancy), respectively, for crystals **I** and **II**. Here, the vacancy concentration increases with an increase in the Zn content, which, in turn, determines the vec of the structure. In general, the vacancy concentration increases with an increase in the Zn content in the γ phase (see Table 5).

This increase of the vacancy concentration with increasing e$^-$/a ratio is well-known in γ-brass-type phases, typical for Hume−Rothery-type compounds.[10,12,27,40,41] These nonstoichiometric vacancies play a decisive role in lowering the overall vec of the phase to the optimal values of ca. 1.615 e$^-$/a because the vacancy is treated as an atomic site with 0 valence electrons. When the vec of a particular γ phase exceeds the critical value for stability, the species can distort structurally, it can remove some atoms such that vec achieves optimal values, or it can achieve both. For instance, γ-Cu$_9$Ga$_4$[42] and γ-Cu$_9$Al$_4$[27] adopt primitive (P-type) cubic structures consisting of two different γ clusters per unit cell. As the Ga or Al concentration in these phases increases, i.e., as vec increases, these structures undergo a rhombohedral distortion, with additional vacancies on the OT and CO sites for Cu$_9$Ga$_4$ and the IT and OH sites for Cu$_9$Al$_4$ related. In Cu$_9$Al$_4$, the IT and OH positions are occupied by Cu atoms. These P-type γ-brass structures tolerate a certain concentration of vacancies before the structural distortion occurs. On the other hand, no symmetry reduction from cubic is evident for the 2 × 2 × 2 superstructure of γ brasses, i.e., F cell or γ' type, although a significant number of nonstoichiometric vacancies are observed in these structures.[10,12,40]

For example, γ' brasses in the Pd−Zn−Al system accommodate structural disorder and vacancies that account for a considerable phase width.[10] On the Zn-rich side, the γ' structure contains 416 atoms per cell, whereas the Al-rich γ' structure contains only 400 atoms because one set of OT sites is completely vacant.[10]

In analogy to other rhombohedrally distorted brasses, the structures of γ-$Au_{5-x}Zn_{8+y}$ can be described by condensed chains of face-sharing icosahedra along the *c* axis. There are two types of icosahedra: (i) Zn1-centered $(M,Au)_{12}$ icosahedra, i.e., Zn1@(M6, Au6); (ii) M3-centered $(M)_{12}$ icosahedra, each of which alternates along the *c* axis. Furthermore, the Zn1-centered icosahedra are surrounded by pentagonal dodecahedra Zn1@[$(M6,Au6)_{12}$@(M3M5M9)8(Zn8)12], with distances ranging from 3.918 to 4.437 Å between the cluster center and dodecahedra. These dodecahedra also form chains along the *c* direction through corner-sharing via the M3 atoms and vertex-sharing along [110] to form a 3D network, as shown in Figure 6c.

Electronic Structure Analysis. The total energies of rhombohedral and cubic γ-brass structures using "Au_5Zn_8" as a model composition were calculated using the Vienna ab initio simulation package (VASP).[43−46] All VASP calculations were performed using projected augmented-wave pseudopotentials[47] with a cutoff energy of 450 eV. A conjugated algorithm was applied for the structural optimization with a 7 × 7 × 7 Monkhorst-pack *k*-points grid to sample the first Brillouin zone (BZ) for reciprocal space integrations.[48] To calculate the total energy, an ordered structure model "Au_5Zn_8" was taken; i.e., mixed sites are treated by either Zn or Au depending upon the relative occupancies on the crystallographic site, and vacancies are not taken into account (for details, see the LMTO-ASA section). Several models were constructed with rhombohedral angle α ranges from 89.68° to 90.06°. During structure optimization, only the atomic coordinates were optimized while keeping the cell volume constant for all models.

The calculated energies of cubic and various rhombohedrally distorted γ-"Au_5Zn_8" models revealed that rhombohedrally distorted structures are energetically more favorable than the cubic phase. Although the energy differences are not very large (36 meV/52 atoms), VASP calculations predicted the observed ground-state structure. The small difference in energies between the cubic and rhombohedral models could be attributed to the absence of vacancies and mixed Au/Zn position for the models, features that are critical components that contribute significantly to the stability of γ-Au_5Zn_8.[10,12] To verify the credibility of VASP for these questions, similar calculations were performed on the well-ordered γ-Cu_5Zn_8. Interestingly, the results show that the cubic structure is energetically more favorable compared to the rhombohedrally distorted γ phase (20 meV/52 atoms), a result that is consistent with experiment. Overall, VASP predicts the observed ground-state structures for both "Au_5Zn_8" and Cu_5Zn_8.

The Stuttgart tight-binding, linear-muffin-tin orbital (TB-LMTO)[49−52] program with the atomic sphere approximation (ASA) was utilized to calculate the DOS and crystal orbital Hamiltonian population (COHP) curves for the rhombohedral structure of "Au_5Zn_8", as a hypothetical representative of the entire γ-phase region. Exchange and correlation were treated in the local density approximation.[53] All relativistic effects except spin−orbit coupling were taken into account by using the scalar relativistic approximation.[54] In the ASA, space is filled with small overlapping Wigner−Seitz (WS) spheres at each atomic site. The symmetry of the potential is considered to be spherical inside each WS sphere, and a combined correction takes into account the overlapping part.[55] The radii of the WS spheres were obtained by requiring that the overlapping potential be the best possible approximation to the full potential and were determined by an automatic procedure.[55] Three empty spheres were introduced to satisfy the LMTO volume criterion. One of the empty spheres was located close to the center of the IT, and the other two were positioned at the centers of triangular faces of the COs (along the 3-fold direction). The corresponding WS radii for the various atoms include the following ranges: Au, 1.494−1.621 Å; Zn, 1.465−1.578 Å; empty spheres, 0.666−0.785 Å. The basis set included Au 6s, 6p, and 5d orbitals and Zn 4s and 4p orbitals (3d orbitals treated as a core function). The *k*-space integrations were accomplished by the tetrahedron method.[56] The self-consistent charge density was obtained by using 364 irreducible *k*-points in the BZ for the rhombohedral cell.

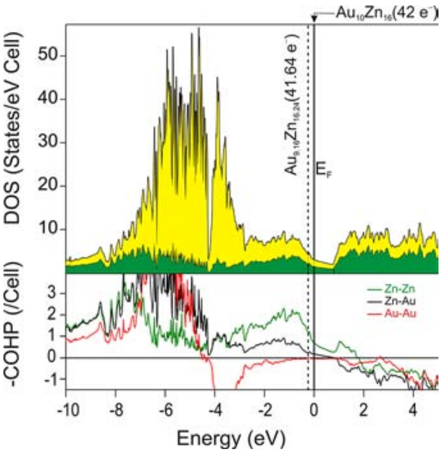

Figure 7. Total DOS (top) and COHP (bottom) curves for the "Au_5Zn_8" structure. The Zn 3d orbitals are not included in either curve. The Zn and Au partial DOSs are shown in green and yellow, respectively.

The calculations were performed on stoichiometric "Au_5Zn_8" as a representative composition of the title compound with the M3 and M8 sites assigned to Au and the M2, M5, and M7 sites assigned to Zn. The above model gives the lowest total energy compared to Au and Zn distributions resembling that of Cu_5Zn_8. To conduct this comparison, the WS radii for Au and Zn were kept constant for the two different models. Although the M8 site shows a slight enrichment of Zn from single-crystal refinements (for **I**, Zn:Au = 61:39), this position is assigned to Au because this gives a better approximation to "Au_5Zn_8" as a representative composition. Moreover, assigning the M8 sites to Zn does not change the nature of the DOS curves. The calculated DOS and COHP curves are shown in Figure 7. The Fermi levels for the observed phases are indicated by solid lines, which fall in a clear pseudogap, as seen from other calculations on γ-brass structures, for example, γ-Cu_5Zn_8 and γ-Cu_9Al_4.[57] Significant contributions to the DOS at the Fermi level come from Zn 4s, Zn 4p, and Au 6p orbitals, while the contribution from Au 6s orbitals is nearly zero. The valence s and p orbitals of Zn and Au show nearly free-electron-like parabolic bands. Other major contributors to the DOS at approximately 5 eV below the Fermi level are the Au 5d states. The pseudogap at the Fermi level is a signature of γ brasses and related Hume−Rothery phases and is also observed for quasicrystal approximant structures.[58] The formation of the pseudogap is due to interactions between the spherical Fermi surface in the free-electron model and faces of the first BZ.[13] However, in the case of γ-Cu_5Zn_8, the distribution of Zn and Cu, respectively, on the IT and OT sites gives rise to ordered polar-covalent, metal−metal interactions that enhance the pseudogap at the Fermi level.[14] In our models of γ-Au_5Zn_8, a similar coloring of the IT and OT sites by Zn and Au also reveals a deep pseudogap. Further computational studies of different coloring patterns are warranted to examine the effect of atomic decorations on the nature of pseudogaps in such complex intermetallic phases.

COHP values were also calculated for "Au_5Zn_8" to elucidate significant orbital interactions within the structure. Figure 7 illustrates the COHP curves for Zn−Zn, Zn−Au, and Au−Au interactions for "Au_5Zn_8". The Au−Au interaction shows nonbonding interactions within the pseudogap region of the DOS, whereas Zn−Zn and Zn−Au remain weakly bonding. The homoatomic Au−Au and Zn−Zn interactions are optimized around 0.8 eV, which corresponds to a valence electron count of 44 e^-/26 atoms, i.e., 1.69 e^-/a or "Au_8Zn_{18}". According to a rigid-band approximation, the anticipated upper limit of Au−Zn γ brasses could be "Au_4Zn_9". However, our experimental studies show that the γ phase extends up to $Au_{4.27}Zn_{8.26}$ and involves nonstoichiometric vacancies at specific crystallographic sites in their structures. Further investigations into the relationship between the vacancy location and concentration in γ brasses are warranted and are currently underway. In order to extend the composition up to Au_8Zn_{18}, the structure needs to accommodate more vacancies that could destabilize the γ phase.

■ SUMMARY

The Au−Zn γ-brass region was investigated by means of synthetic, structural, thermal, and theoretical analysis. Au−Zn γ phases adopt a rhombohedrally distorted γ-brass-type structure with a noticeable phase width assigned from 60.0 to 66.0 atom % Zn at 300 °C based on the single-crystal and EDS analysis. Thus, the stability of Au−Zn γ phases occurs for vec values between 1.61 and 1.66 e^-/a. Furthermore, vacancies on the OT and OH sites of the 26-atom γ cluster play a critical role in keeping vec of the Au−Zn γ phases to optimal values, which fall well within the expected range for a γ-brass structure. During this investigation, we also discovered a new phase with approximate unit-cell composition $Au_{72.5}Zn_{150}$, which crystallizes in trigonal symmetry. Powder XRD indicates that the γ phase coexists with either β' or $Au_{72.5}Zn_{150}$, depending on the loaded composition. In addition, we also confirmed the existence of the γ_2 phase, $AuZn_3$. Overall, our experimental results agree in large part with the phase diagram reported by Okamoto and Massalski.[16] However, further studies are required to estimate accurate phase width and thermal stability of the new $Au_{72.5}Zn_{150}$ phase, and these investigations are in progress.

■ ASSOCIATED CONTENT

Supporting Information

X-ray crystallographic data in CIF format, Tables S1−S7, and Figures S1−S8. This material is available free of charge via the Internet at http://pubs.acs.org.

■ AUTHOR INFORMATION

Corresponding Author

*E-mail: srini@iastate.edu.

Notes

The authors declare no competing financial interest.

■ ACKNOWLEDGMENTS

This work was carried out at Ames Laboratory, which is operated for the U.S. Department of Energy by Iowa State University under Contract DE-AC02-07CH11358. This work was supported by the U.S. Department of Energy, Office of Basic Energy Sciences, Division of Materials Sciences and Engineering.

■ REFERENCES

(1) Mizutani, U. *Hume−Rothery Rules for Structurally Complex Alloy Phases*; CRC Press, Taylor & Francis Group: Boca Raton, FL, 2011.
(2) Mizutani, U.; Asahi, R.; Sato, H.; Takeuchi, T. *Philos. Mag.* **2006**, *86*, 645.
(3) Mizutani, U.; Noritake, T.; Ohsuna, T.; Takeuchi, T. *Philos. Mag.* **2010**, *90*, 1985.
(4) Gourdon, O.; Miller, G. J. *Chem. Mater.* **2006**, *18*, 1848.
(5) Gourdon, O.; Izaola, Z.; Elcoro, L.; Petricek, V.; Miller, G. J. *Inorg. Chem.* **2009**, *48*, 9715.
(6) Belin, C. H. E.; Belin, R. C. H. *J. Solid State Chem.* **2000**, *151*, 85.
(7) Morton, A. J. *Acta Metall.* **1979**, *27*, 863.
(8) Gross, N.; Kotzyba, G.; Künnen, B.; Jeitschko, W. *Z. Anorg. Allg. Chem.* **2001**, *627*, 155.
(9) Thimmaiah, S.; Conrad, M.; Lee, S.; Harbrecht, B. *Z. Anorg. Allg. Chem.* **2004**, *630*, 1762.
(10) Thimmaiah, S.; Miller, G. J. *Chem.—Eur. J.* **2010**, *16*, 5461.
(11) Thimmaiah, S.; Miller, G. J. *Acta Crystallogr., Sect. E* **2010**, *66*, i5.
(12) Thimmaiah, S.; Crumpton, N. A.; Miller, G. J. *Z. Anorg. Allg. Chem.* **2011**, *637*, 1992.
(13) Paxton, A. T.; Methfessel, M.; Pettifor, D. G. *Proc. R. Soc. London, Ser. A* **1997**, *453*, 1493.
(14) Gourdon, O.; Gout, D.; Williams, D. J.; Proffen, T.; Hobbs, S.; Miller, G. J. *Inorg. Chem.* **2006**, *46*, 251.
(15) Mott, N. F.; Jones, H. *The Theory of the Properties of Metals and Alloys*; Courier Dover Publications: North Chemsford, MA, 1958.
(16) Okamoto, H.; Massalski, T. *J. Phase Equilib.* **1989**, *10*, 59.
(17) Okamoto, H. *J. Phase Equilib.* **2006**, *27*, 427.
(18) Pearson, W. B. *J. Less-Common Met.* **1979**, *68*, P9.
(19) Ipser, H.; Krachler, R. *Scr. Metall.* **1988**, *22*, 1651.
(20) Günzel, E.; Schubert, K. *Z. Metallkd.* **1958**, *49*, 234.
(21) Maciolek, R. B.; Mullendore, J. A.; Dodd, R. A. *Acta Metall.* **1967**, *15*, 259.
(22) Brandon, J. K.; Pearson, W. B.; Riley, P. W.; Chieh, C.; Stokhuyzen, R. *Acta Crystallogr.* **1977**, *B33*, 1088.
(23) Liu, H. S.; Ishida, K.; Jin, Z. P.; Du, Y. *Intermetallics* **2003**, *11*, 987.
(24) Gourdon, O.; Bud'ko, S.; Williams, D.; Miller, G. J. *Inorg. Chem.* **2004**, *43*, 3210.
(25) Gourdon, O.; Miller, G. J. *J. Solid State Chem.* **2003**, *173*, 137.
(26) Ellner, M. *Metall. Mater. Trans. A* **1990**, *21*, 1669.
(27) Kisi, E. H.; Browne, J. D. *Acta Crystallogr., Sect. B* **1991**, *B47*, 835.
(28) Lindahl, T.; Westman, S. *Acta Chem. Scand.* **1969**, *23*, 1181.
(29) Ko, H.; Gourdon, O.; Gout, D.; Mun, E.-D.; Thimmaiah, S.; Miller, G. J. *Inorg. Chem.* **2010**, *49*, 11505.
(30) *WinXPow 3.0.1.11*; Stoe & Cie GmbH: Darmstadt, Germany, 2010.
(31) *SMART*; Bruker AXS, Inc.: Madison, WI, 1997−2005.
(32) *SHELXTLPlus*, version 6.14; Bruker AXS, Inc.: Madison, WI, 2003.
(33) Hamilton, W. *Acta Crystallogr.* **1965**, *18*, 502.
(34) Thimmaiah, S.; Miller, G. J. To be published.

(35) Ipser, H.; Mikula, A.; Terzieff, P. *Monatsh. Chem.* **1983**, *114*, 1177.
(36) Bärnighausen, H. *Commun. Math. Chem.* **1980**, *9*, 139.
(37) Wondratschek, H.; Müller, U. *International Tables for Crystallography, Vol. A1: Symmetry Relations between Space Groups*; Springer: Berlin, 2008.
(38) Bradley, A. J.; Thewlis, J. *Proc. R. Soc. London* **1926**, *112A*, 678.
(39) Gourdon, O.; Miller, G. *J. Chem. Mater.* **2006**, *18*, 1848.
(40) Thimmaiah, S.; Richter, K. W.; Lee, S.; Harbrecht, B. *Solid State Sci.* **2003**, *5*, 1309.
(41) Harbrecht, B.; Thimmaiah, S.; Armbrüster, M.; Pietzonka, C.; Lee, S. *Z. Anorg. Allg. Chem.* **2002**, *628*, 2744.
(42) Mizutani, U.; Noritake, T.; Ohsuna, T.; Takeuchi, T. *Philos. Mag.* **2010**, *90*, 1985.
(43) Kresse, G.; Furthmüller, J. *Comput. Mater. Sci.* **1996**, *6*, 15.
(44) Kresse, G.; Furthmüller, J. *Phys. Rev. B* **1996**, *54*, 11169.
(45) Kresse, G.; Hafner, J. *Phys. Rev. B* **1993**, *47*, 558.
(46) Kresse, G.; Hafner, J. *Phys. Rev. B* **1994**, *49*, 14251.
(47) Kresse, G.; Joubert, D. *Phys. Rev. B* **1999**, *59*, 1758.
(48) Monkhorst, H. J.; Pack, J. D. *Phys. Rev. B* **1976**, *13*, 5188.
(49) Andersen, O. K. *Phys. Rev.* **1975**, *B12*, 3060.
(50) Andersen, O. K. *Phys. Rev.* **1986**, *B34*, 2439.
(51) Andersen, O. K.; Jepsen, O. *Phys. Rev. Lett.* **1984**, *53*, 2571.
(52) Andersen, O. K.; Jepsen, O.; Glötzel, D.; Bassani, F.; Fumi, F.; Tosi, M. P.; Lambrecht, W. R. L. *Highlights of Condensed-Matter Theory*; North Holland Publishers: Amsterdam, The Netherlands, 1985.
(53) Von Barth, U.; Hedin, L. *J. Phys. C* **1972**, *5*, 1629.
(54) Koelling, D. D.; Harmon, B. N. *J. Phys. C* **1977**, *10*, 3107.
(55) Jepsen, O.; Andersen, O. K. *Z. Phys. B* **1995**, *97*, 35.
(56) Blöchl, P. E.; Jepsen, O.; Andersen, O. K. *Phys. Rev.* **1994**, *B49*, 16223.
(57) Asahi, R.; Sato, H.; Takeuchi, T.; Mizutani, U. *Phys. Rev. B* **2005**, *71*, 165103.
(58) Takeuchi, T.; Sato, H.; Mizutani, U. *J. Alloys Compd.* **2002**, *342*, 355.
(59) Brandon, J. K.; Brizard, R. Y.; Chieh, P. C.; McMillan, R. K.; Pearson, W. B. *Acta Crystallogr., Sect. B* **1974**, *30*, 1412.